Atmos. Chem. Phys. Discuss., https://doi.org/10.5194/acp-2018-1299
Manuscript under review for journal Atmos. Chem. Phys.
Discussion started: 14 January 2019

Atmospheric Chemistry and Physics Discussions

Investigation of Arctic middle-atmospheric dynamics using 3 years of H_2O and O_3 measurements from microwave radiometers at Ny-Ålesund

Franziska Schranz[1], Brigitte Tschanz[1], Rolf Rüfenacht[1,a], Klemens Hocke[1], Mathias Palm[2], and Niklaus Kämpfer[1]

[1]Institute of Applied Physics, University of Bern, Bern, Switzerland
[2]Institute of Environmental Physics, University of Bremen, Bremen, Germany
[a]now at: Federal Office for Meteorology and Climate MeteoSwiss, Payerne, Switzerland

Correspondence: Franziska Schranz (franziska.schranz@iap.unibe.ch)

Abstract.

We use 3 years of water vapour and ozone measurements to analyse dynamical events in the polar middle atmosphere such as sudden stratospheric warmings (SSW), polar vortex shifts, water vapour descent rates and periodicities. The measurements were performed with the two ground-based microwave radiometers MIAWARA-C and GROMOS-C which are co-located at the AWIPEV research base at Ny-Ålesund, Svalbard (79° N, 12° E) since September 2015. The almost continuous datasets of water vapour and ozone are characterised by a high time resolution in the order of hours. A thorough intercomparison of these datasets with models and measurements from satellite, ground-based and in-situ instruments was performed. In the upper stratosphere and lower mesosphere the MIAWARA-C profiles agree within 5 % with SD-WACCM simulations and ACE-FTS measurements whereas AuraMLS measurements show an average offset of 10–15 % depending on altitude but constant in time. Stratospheric GROMOS-C profiles are within 5 % of the satellite instruments AuraMLS and ACE-FTS and the ground-based microwave radiometer OZORAM which is also located at Ny-Ålesund. During these first three years of the measurement campaign typical phenomena of the Arctic middle atmosphere took place and we analysed their signatures in the water vapour and ozone datasets. Inside of the polar vortex in autumn we found the descent rate of mesospheric water vapour to be 435 m/day on average. In early 2017 distinct increases in mesospheric water vapour of about 2 ppm were observed when the polar vortex was displaced and midlatitude air was brought to Ny-Ålesund. Two major sudden stratospheric warmings took place in March 2016 and February 2018 where ozone enhancements of up to 4 ppm were observed. The zonal wind reversals accompanying a major SSW were captured in the GROMOS-C wind profiles which are retrieved from the ozone spectra. After the SSW in February 2018 the polar vortex re-established and the water vapour descent rate in the mesosphere was 355 m/day. In the water vapour and ozone time series signatures of atmospheric waves with periods close to 2, 5, 10 and 16 days were found.

Atmos. Chem. Phys. Discuss., https://doi.org/10.5194/acp-2018-1299
Manuscript under review for journal Atmos. Chem. Phys.
Discussion started: 14 January 2019

Atmospheric Chemistry and Physics Discussions

1 Introduction

In the Arctic middle atmosphere the solar irradiation conditions change dramatically throughout the year. These seasonal insolation changes drive the typical summer and winter pattern in the atmospheric dynamics and the photochemistry of trace species in the polar stratosphere and mesosphere. In winter, during the polar night, middle atmospheric air is descending and a cyclonic wind system, the polar vortex, dominates the middle atmospheric dynamics and builds a mixing barrier between Arctic and midlatitude air. In summer, when the sun never sets, airmasses are rising and an anticyclone forms around the pole, which is however much weaker than the winter polar vortex.

Ny-Ålesund is located at 79°N and is therefore the ideal location to perform observations in the polar middle atmosphere. In winter Ny-Ålesund is mostly located inside of the polar vortex but the vortex shifts off the pole frequently during midwinter and therefore observations in and outside of the polar vortex are possible. Many phenomena related to the dynamics of the polar vortex can be observed from this high latitude location. The most dramatic events which occur in the polar winter atmosphere are sudden stratospheric warmings (SSW). The events couple all atmospheric layers (Baldwin and Dunkerton, 2001; Funke et al., 2010) and lead to temperature increases of more than 25 K within a few days and zonal wind reversals in the stratosphere, whereas the temperature decreases in the mesosphere. The polar vortex is thereby shifted or even splits in two or more sub-vortices. Global-scale planetary waves can interact with the mean flow in the middle atmosphere and influence the large scale circulation. The wave–mean-flow interaction is believed to be the main cause of SSWs (Matsuno, 1970; Liu and Roble, 2002). Within the winter polar vortex mesospheric and stratospheric air descends and transports chemical constituents to lower altitudes. This includes long lived constituents which were produced during solar proton events at high altitudes like NOx and which lead to stratospheric ozone destructions of 10 % (Denton et al., 2017, 2018). In this article we focus on the analysis of dynamical events in the polar middle atmosphere as seen from Ny-Ålesund using water vapour and ozone data from ground-based microwave radiometers.

Water vapour is a valuable tracer for transport in the Arctic middle atmosphere. It has a lifetime in the order of weeks in the upper mesosphere and in the order of months in the lower mesosphere (Brasseur and Solomon, 2005) which is long compared to the timescales of dynamical processes. Additionally it has vertical and horizontal gradients in its volume mixing ratio (VMR). The vertical gradient is positive in the stratosphere because of the water vapour production through photodissociation of methane in the middle atmosphere. In the mesosphere it is negative because water vapour is photodissociated through the absorption of Lyman-α radiation (Brasseur and Solomon, 2005). The horizontal gradients occur in winter. Airmasses descend within the polar vortex and in the absence of solar irradiation the water vapour maximum descends with it. This leads to a positive gradient across the vortex edge in the stratosphere and a negative gradient in the mesosphere. Water vapour has previously been used as a tracer to study dynamical events like periodicities, transport during SSWs and descent rates within the polar vortex (Tschanz and Kämpfer, 2015; Bailey et al., 2014; Straub et al., 2012; Scheiben et al., 2012; Lee et al., 2011).

Stratospheric ozone can be used as a tracer of horizontal transport processes in winter where odd oxygen is under dynamical control and ozone has a strong gradient across the polar vortex edge. It can therefore be used to distinguish air parcels from

Atmos. Chem. Phys. Discuss., https://doi.org/10.5194/acp-2018-1299
Manuscript under review for journal Atmos. Chem. Phys.
Discussion started: 14 January 2019

in and outside of the polar vortex. Together with water vapour it was used as a tracer for vortex filamentation in the lower stratosphere (Müller et al., 2003) and Atlantic streamers (Hocke et al., 2017).

Observations of water vapour and ozone in the Arctic middle atmosphere are rare. Therefore it was decided to place the two ground-based microwave radiometers MIAWARA-C and GROMOS-C in the Arctic. Ground-based microwave radiometry is the ideal technique to monitor water vapour and ozone in the middle atmosphere. It allows a continuous observation under all weather conditions except during heavy rain and a high time resolution in the order of hours. GROMOS-C and MIAWARA-C are specially designed for campaigns and are therefore compact, easy to maintain and remote controlled. In the Arctic MIAWARA-C is the only ground-based instrument continuously measuring middle atmospheric water vapour profiles except for the radiometer Vespa22 (Mevi et al., 2018) located at Thule, Greenland. Ozone profiles in the Arctic middle atmosphere are measured with GROMOS-C and with OZORAM (Palm et al., 2010) which is also located at Ny-Ålesund. The additional benefit of GROMOS-C is that it provides ozone measurements down to about 20 km and zonal and meridional wind profiles.

In this article we investigate dynamical events in the Arctic middle atmosphere like sudden stratospheric warmings (SSW), polar vortex shifts, water vapour descent rates within the polar vortex in autumn and periodicities. For the analysis we use 3 years of almost continuous water vapour and ozone volume mixing ratio (VMR) measurements in the middle atmosphere above Ny-Ålesund (79°N) in the Arctic. The measurements were performed with the two ground based microwave radiometers MIAWARA-C and GROMOS-C and have a high time resolution in the order of hours. Additionally a thorough intercomparison with models, satellite measurements and co-located ground-based and in-situ measurements from Ny-Ålesund was performed.

The remainder of this article is organised as follows: An introduction to the campaign at Ny-Ålesund is given in Sect. 2. In Sect. 3 the ground based microwave radiometers MIAWARA-C and GROMOS-C are described in detail as well as the instruments and models used for intercomparison. The water vapour and ozone datasets of the microwave radiometers MIAWARA-C and GROMOS-C are described in Sect. 4 and a comprehensive intercomparison with other instruments and models is presented in Sect. 5. In the following sections we report on typical phenomena of the Arctic middle atmosphere as observed in the water vapour, ozone and wind time series from Ny-Ålesund: the descent of air in the polar vortex during its formation (Sect. 6), vortex shifts (Sect. 7), sudden stratospheric warmings (Sect. 8) and periodicities (Sect. 9). Summary and conclusion are given in Sect. 10.

2 Ny-Ålesund Campaign

Within the frame of the Ny-Ålesund campaign MIAWARA-C and GROMOS-C, two ground-based microwave radiometers of the University of Bern, were moved to the AWIPEV research base at Ny-Ålesund/Svalbard (79° N, 12° E) in September 2015. Currently the instruments have been measuring water vapour and ozone VMR profiles at Ny-Ålesund for 3 years and the campaign is ongoing. This campaign is a collaboration with the University of Bremen which operates the ozone radiometer OZORAM at Ny-Ålesund since 1994. All instruments belong to the Network for the Detection of Atmospheric Composition Change (NDACC, De Mazière et al. (2018)).

Atmos. Chem. Phys. Discuss., https://doi.org/10.5194/acp-2018-1299
Manuscript under review for journal Atmos. Chem. Phys.
Discussion started: 14 January 2019

The aim of the campaign is to study the variability and possible anti-correlation between water vapour and ozone and to investigate dynamical and chemical phenomena in the polar middle atmosphere. Diurnal ozone variations and their seasonal differences have already been investigated (Schranz et al., 2018). In this article we present the water vapour and the ozone datasets of MIAWARA-C and GROMOS-C and we concentrate on analysing the traces of dynamical events in both water vapour and ozone. A possibility for the future would be to investigate spatial ozone variations from the measurements in the four cardinal directions or the effects of energetic particle precipitation on the water vapour and ozone concentration.

3 Instruments and Models

3.1 MIAWARA-C

MIAWARA-C, the MIddle Atmospheric WAter vapour RAdiometer for Campaigns, is a ground based microwave radiometer built at the University of Bern and specially designed for campaigns. It is therefore a very compact instrument which only needs a power- and an internet-connection and which is operated remotely. The instrument front end is an uncooled heterodyne receiver with a system temperature of 150 K. In the back end the signal is spectrally analysed with an FFT spectrometer with 400 MHz bandwidth and 30.5 kHz spectral resolution. The instrument measures the pressure broadened emission line of water vapour at 22 GHz. The retrieval of the water vapour profiles from the spectra is performed with QPACK (Eriksson et al., 2005) and ARTS2 (Eriksson et al., 2011), using an optimal estimation method (Rodgers, 1976). An a priori water vapour profile is required for the optimal estimation method and is taken from an MLS climatology of the years 2004–2008. The retrieved water vapour profiles have an altitude range of 37–75 km with a vertical resolution of 12–19 km. For MIAWARA-C retrievals with a constant time resolutions (6h, 12h and 24h) and with a constant noise level of 0.014 K are performed. For the constant noise level retrieval the integration time depends on the tropospheric opacity and ranges from 30 minutes to more than 1 day. For 80 % of the retrievals the integration time is below 2 hours. Detailed descriptions of the instrument can be found in Straub et al. (2010) and Tschanz et al. (2013).

MIAWARA-C has been located at Bern (47° N, 7°E) and Sodankylä (67° N, 27° E) in the years 2010–2013 where a comprehensive intercomparison was performed and the mean bias to satellites and other ground-based microwave radiometers was calculated (Tschanz et al., 2013). With respect to MLS version 3.3, there is almost no bias at the lowest altitude level (4 hPa) but an increasing dry bias with higher altitudes of up to -13 % at 0.02 hPa.

3.2 GROMOS-C

GROMOS-C, the GRound-based Ozone MOnitoring System for Campaigns, is a microwave radiometer built at the University of Bern. Similarly to MIAWARA-C it is a campaign instrument and the design is very compact. It needs a power- and an internet-connection and is then controlled remotely. The instrument has an uncooled heterodyne receiver system with a system temperature of 1080 K. The spectral analysis of the signal is performed with a FFT spectrometer of 1 GHz bandwidth and a spectral resolution of 30.5 kHz. In its basic mode GROMOS-C measures the pressure broadened emission line of ozone at

110.8 GHz. It can however switch to measure the CO-line at 115.3 GHz. Additionally it is possible to retrieve wind profiles from the ozone spectra according to the measurement principle of Rüfenacht et al. (2012) and Rüfenacht and Kämpfer (2017). Therefore GROMOS-C observes subsequently in the four cardinal directions (N-E-S-W) at 22° elevation with a sampling time of 4 seconds. At the Arctic location of Ny-Ålesund this allows observations in and outside of the polar vortex if the vortex edge is close to Ny-Ålesund (Schranz et al., 2018). The retrieval of ozone and wind is performed with Qpack (Eriksson et al., 2005) and ARTS2 (Eriksson et al., 2011), using an optimal estimation method (Rodgers, 1976). For ozone the a priori is taken from an MLS climatology of the years 2004–2013 whereas a zero a priori with relatively large variance is used for wind. The ozone profiles of GROMOS-C have an altitude range of 20–70 km with a vertical resolution of 10–12 km in the stratosphere and up to 20 km in the mesosphere. The time resolution is 2 hours. Detailed information about the instrument can be found in Fernandez et al. (2015).

A validation campaign took place at La Reunion in 2014 and revealed that GROMOS-C and MLS ozone measurements agree within 5 % up to 0.2 hPa. (Fernandez et al., 2016).

3.3 OZORAM

OZORAM, the OZone Radiometer for Atmospheric Measurements, is a ground-based microwave radiometer built at the University of Bremen. The instrument is located at Ny-Ålesund since 1993 and is in its current observation mode since 2008. It has a heterodyne receiver system and the signal is then spectrally analysed with an FFT spectrometer with 800 MHz bandwidth and a spectral resolution of 60 kHz. OZORAM measures the pressure broadened ozone emission line at 142 GHz. For the retrieval of the ozone profiles from the measured spectra ARTS 1.1 (Buehler et al., 2005) is used together with QPACK (Eriksson et al., 2005). The profiles have an altitude range of 30–70 km with a vertical resolution of 10–20 km and a time resolution of 1 h.

A detailed description of the instrument can be found in Palm et al. (2010) where also an intercomparison with the satellite instruments MLS and SABER was performed. OZORAM is within 10 % of MLS and SABER in the stratosphere and within 30 % in the mesosphere.

3.4 MLS

The Microwave Limb Sounder (MLS) is an instrument on board NASA's Aura satellite which was launched in 2004 (Waters et al., 2006). The satellite is in a sun synchronous orbit at 705 km altitude and with 98° inclination. It passes a given location on the Earth surface two times a day. At Ny-Ålesund it measures at around 04:00 and 10:00 UTC. Water vapour is retrieved from the 183 GHz line and ozone from the 240 GHz band. It provides ozone profiles from 12–80 km altitude and water vapour from 5–80 km altitude. The vertical resolution is 2.7–5 km. Profiles for comparison are selected if their location is within $\pm 1.2°$ latitude and $\pm 6°$ longitude from Ny-Ålesund. For this study we use the retrieval version 4.2.

In the SPARC water vapour assessment (Nedoluha et al., 2017) the MLS water vapour data set was intercompared to ground-based microwave radiometers from all over the world. The study showed that MLS water vapour profiles are typically 0-10 % higher than the profiles from the microwave radiometers in the range of 3–0.03 hPa. MLS ozone profiles were intercompared to

ground-based microwave radiometer measurements at the NDACC sites Lauder, New Zealand and Mauna Loa, Hawaii (Boyd et al., 2007). The profiles agree within 5 % in the range of 18–0.04 hPa.

3.5 ACE-FTS

ACE-FTS is a high resolution infrared Fourier Transform Spectrometer and the main instrument of the Canadian Atmospheric Chemistry Experiment satellite mission which is also called SCISAT (Bernath, 2017). The satellite is in a 73.9° orbit at 650 km altitude. ACE-FTS performs solar occultation measurements from 2.2–13.3μm. The retrieved profiles have an altitude range of 5–95 km for ozone and 5–101 km for water vapour and an altitude resolution of 3–4 km. Within 3 years ACE measured only 6 profiles which were within ±2° latitude and ±4° longitude of Ny-Ålesund. For this study we use data from the retrieval version 3.6.

A global intercomparison of ACE-FTS ozone and water vapour profiles with MLS and MIPAS profiles revealed an average bias of -5 % between 20–60 km for water vapour. ACE-FTS ozone profiles are within ±5 % of MLS and MIPAS profiles in the mid stratosphere and exhibit a positive bias of 10–20 % in the upper stratosphere and lower mesosphere (Sheese et al., 2017).

3.6 SD-WACCM

The Whole Atmosphere Community Climate Model (WACCM) (Marsh et al., 2013) is the "high-top" atmospheric component of NCAR's Community Earth System model (CESM). It is based on the Community Atmosphere Model (CAM, Collins et al. (2006)) and the chemistry module is taken from the Model for Ozone and Related Chemical Tracers (MOZART, Emmons et al. (2010)). For this study we use the specified dynamics version of WACCM (SD-WACCM, Brakebusch et al. (2013)) within CESM version 1.2.2. The model spans from ground to an altitude of 145 km with 88 levels and a vertical resolution of 0.5–4 km. It has a horizontal resolution of 1.9° latitude and 2.5° longitude and a time resolution of 30 minutes. In the specified dynamics version horizontal winds, temperature, surface wind stress, surface pressure and specific and latent heat flux are nudged with GEOS5 analysis data (Rienecker et al., 2008). The nudging is performed at every time step with a strength of 10 % and up to an altitude of 60 km. Hoffmann et al. (2012) has shown that the nudging, although only 10 % and up to 60 km altitude, yields realistic variations of carbon monoxide (CO) in the higher mesosphere.

3.7 ERA5

ERA5 (Copernicus Climate Change Service (C3S), 2017; Hersbach and Dee, 2016) is a climate re-analysis of the European Center for Medium Range Weather Forecast (ECMWF). For its production a 4D Var data assimilation scheme was used in the Integrated Forecast System (IFS Cycle 41r2). ERA5 provides hourly analysis fields at a horizontal resolution of 31 km and from the surface up to 0.01 hPa (about 80km). The vertical resolution is 20m–2.5km.

Atmos. Chem. Phys. Discuss., https://doi.org/10.5194/acp-2018-1299
Manuscript under review for journal Atmos. Chem. Phys.
Discussion started: 14 January 2019

3.8 Ozone radiosonde

Balloon-borne ozone radiosondes are launched once per week at 11 UT from the AWIPEV station at Ny-Ålesund. During polar night the launch frequency is enhanced to two sondes per week and during measurement campaigns even to one sonde per day. The used ozone sensor is an electrochemical concentration cell (ECC) model 6A. The weather balloons which carry the ozone sondes reaches altitudes of about 30 km within 1 h 40 min. A measurement is performed every 5 seconds which leads to an average vertical resolution of 30 m.

4 H_2O and O_3 data sets of MIAWARA-C and GROMOS-C

The ground-based microwave radiometers MIAWARA-C and GROMOS-C gathered a 3 year long and almost continuous time series of middle atmospheric water vapour and ozone VMR in the Arctic. The instruments are located at the AWIPEV research station at Ny-Ålesund, Svalbard (79°N, 12°E) and the measurements started in September 2015 and are ongoing.

4.1 H_2O time series of MIAWARA-C

The 3 year long data set of water vapour volume mixing ratio (VMR) measured with MIAWARA-C is presented in Fig.1. It shows a time series of water vapour VMR profiles in the altitude range of 10–0.005 hPa which corresponds approximately to 30–80 km.

The horizontal white lines indicate the upper and lower bound of the trustworthy altitude range. It is defined as the region where the measurement response is larger than 0.8. The measurement response for an altitude level is given by the area below the corresponding averaging kernel. The optimal estimation method, which is used to retrieve a profile out of the measured spectra, needs additional information which is given in the form of an a priori profile. The measurement response is a measure for how large the contribution of the measurement is compared to the contribution of the a priori profile. A measurement response larger than 0.8 means that the measured spectrum contributes more than 80 % to the retrieved VMR. The trustworthy altitude range is larger in winter when the opacity of the troposphere is lower. The vertical grey lines are data gaps which are due to power cuts or rain as MIAWARA-C needs to close its cover when it rains.

The time series shows the annual cycle of water vapour VMR. In the mesosphere at 0.1 hPa water vapour has a maximum in summer of about 7.5 ppm and in winter it decreases to about 3.5 ppm. In the upper stratosphere at 5 hPa the maximum of about 7.5 ppm is seen in autumn when mesospheric water vapour is descending in the winter polar vortex and the minimum of about 6 ppm is seen in spring. The effective descent rate of water vapour during the formation of the polar vortex of the three winters since September 2015 is discussed in section 6. During winter the variability of water vapour is dominated by the dynamics of the polar vortex. Horizontal water vapour VMR gradients across the vortex edge lead to variations in the water vapour mixing ratios above Ny-Ålesund when the vortex moves away from Ny-Ålesund. This is mainly seen during winter 2016/2017 and is discussed in section 7.

Atmos. Chem. Phys. Discuss., https://doi.org/10.5194/acp-2018-1299
Manuscript under review for journal Atmos. Chem. Phys.
Discussion started: 14 January 2019

4.2 O_3 time series of GROMOS-C

Figure 2 presents the time series of ozone VMR measured with GROMOS-C over 3 years. The ozone profiles cover an altitude range of 100–0.03 hPa which corresponds to about 15–70 km. The horizontal white lines indicate the measurement response of 0.8, smoothed over 2 days. Data gaps are indicated with the vertical grey lines. During winter 2017/2018 GROMOS-C measured CO for about 2 months and during winter 2016/2017 the spectrometer had a hardware problem.

The main ozone layer at about 35 km is clearly seen as well as the annual cycle with higher ozone VMR in summer (6 ppm) than in winter (4.5 ppm). Stratospheric ozone VMR above Ny-Ålesund depends on the dynamics of the winter polar vortex. This is seen from January to April 2017 as well as during two major sudden stratospheric warmings in March 2016 and February 2018 where stratospheric ozone VMR reached exceptionally high values of more than 8 ppm (Sect. 8). In the mesosphere a diurnal cycle was detected in spring and autumn whereas in the stratosphere at 10 hPa the diurnal variation is seen in mid summer during the period of polar day (Schranz et al., 2018).

5 Intercomparison

The water vapour and ozone datasets of the two ground-based microwave radiometers of the University of Bern were intercompared with satellite measurements of MLS and ACE and with the models SD-WACCM and ERA5. The ozone time series was additionally intercompared with balloon borne ozone measurements where there was a reasonable overlap in altitude and measurements from the ground-based microwave radiometer OZORAM. The left panels in the Figs. 3 and 5 show the daily mean VMR of all the different datasets averaged within four pressure intervals covering 3–0.03 hPa for water vapour and five pressure intervals covering 30–0.1 hPa for ozone. The time series start in September 2015 and end in September 2018. In the right panel the relative differences of the different datasets to MIAWARA-C and GROMOS-C measurements are shown.

An intercomparison of the profiles was also performed. The time series was divided into bins according to the integration time of MIAWARA-C (6 hours) and GROMOS-C (2 hours). The profiles of the other instruments or models which fall into a bin were then averaged and convolved with the averaging kernels of the instruments and the relative difference between the profiles was calculated. The balloon borne ozone sonde data were not convolved. In Figs. 4 and 6 the median of the relative difference profiles is shown (left) as well as their median absolute deviation from the median (MAD) which is defined as $\mathrm{MAD} = \mathrm{median}_i|x_i - \bar{x}|$ where $\bar{x} = \mathrm{median}_j(x_j)$ as measure for the spread (right).

5.1 H_2O intercomparison

The intercomparison of the MIAWARA-C water vapour time series with measurements of the satellite instruments MLS and ACE as well as with the models SD-WACCM and ERA5 shows that MIAWARA-C and SD-WACCM agree within 10 % in the lowest panel (1-3 hPa) and that the six ACE measurements are even within 5 % (Fig. 3). ERA5 sees less water vapour in late summer but is also mostly within $\pm$10 %. MLS measurements, however, have an offset of about 15 % which is constant over the whole time period and it persists also at the higher altitude levels. With increasing altitude SD-WACCM and ERA5 start to

see less water vapour in winter and more water vapour in early summer than MIAWARA-C. ACE stays close to MIAWARA-C also at higher altitudes, it is however always higher than MIAWARA-C and the ACE measurements cover only the period of end of September until mid October.

The median of the relative difference profiles (Fig. 4) shows that SD-WACCM and ACE are within ±5 % of MIAWARA-C up to 0.1 hPa. MLS has a median offset of 10–15 % whereas for ERA5 the median relative difference is -3– -13 %. Above 0.1 hPa MIAWARA-C starts to see less water vapour than MLS, SD-WACCM and ACE.

An offset of MLS (13 %) was already seen in an earlier intercomparison study of MIAWARA-C at Bern and Sodankylä. In the SPARC water vapour assessment for the years 2004–2015 the offset of MLS to ground-based microwave radiometers is also mentioned (Nedoluha et al., 2017) but the mean relative difference (0–10 %) is smaller than for MIAWARA-C. At Thule, Greenland Mevi et al. (2018) measured water vapour with a ground-based microwave radiometer for 1 year starting in July 2016 and noticed no clear difference to MLS.

5.2 O_3 intercomparison

The ozone time series measured with GROMOS-C is intercompared with satellite data sets of MLS and ACE and with the models SD-WACCM and ERA5 in Fig. 5. In the lowest pressure interval (30–10 hPa) the GROMOS-C measurements are also intercompared to balloon-borne ozone sonde measurements and from 10–0.1 hPa they are additionally compared to the OZORAM measurements. In the lowest panel (30–10 hPa) all models and instruments agree with each other except GROMOS-C which measures up to 20 % higher ozone VMRs in summer. This annual variation persists up to 1 hPa. At 1–0.3 hPa GROMOS-C agrees with OZORAM well within ±10 % whereas SD-WACCM and MLS show lower VMRs. At 0.3–0.1 hPa the relative differences are high due to very low VMRs but the datasets agree well with each other. ERA5 ozone VMR above 3 hPa deviates substantially from the other datasets and is therefore not included in the intercomparison.

Up to 0.5 hPa (about 55) the median of the differences relative to GROMOS-C are mainly within 5 % for OZORAM (above 6 hPa), MLS, ACE, SD-WACCM and ERA5 (Fig. 6). The relative difference of the balloon borne ozone sonde to MIAWARA-C is increasing from -3 % at 30 hPa to -13 % at 10 hPa. In general the ozone measurements of GROMOS-C are up to 5 % higher than OZORAM, MLS, SD-WACCM and ERA5.

6 Effective descent rate of H_2O

Middle atmospheric air at the poles is descending within the polar vortex during its formation in autumn. We determined the effective descent rate of water vapour in the mesosphere above Ny-Ålesund from the MIAWARA-C data and at the latitude of 79° N from the MLS zonal mean data. These descent rates were then compared to the descent rates calculated from the water vapour time series simulated with SD-WACCM and ERA5 at Ny-Ålesund.

To determine the descent rate a linear least squares fit of the 5.5 ppm isopleth was performed between September 15 and November 1 for the years 2015–2017. During these time intervals the mesosphere above Ny-Ålesund was always inside of the

Atmos. Chem. Phys. Discuss., https://doi.org/10.5194/acp-2018-1299
Manuscript under review for journal Atmos. Chem. Phys.
Discussion started: 14 January 2019

Atmospheric Chemistry and Physics Discussions

polar vortex system and the water vapour time series showed a linear descent. The 5.5 ppm isopleths covered a big part of the mesosphere (0.02–0.4 hPa, approximately 73–53 km) within this time interval.

We assumed an uncertainty of 10 % for the MIAWARA-C water vapour VMR measurement and 5 % for the MLS zonal mean. The water vapour VMR in the mesosphere is linearly decreasing with altitude and we can determine the inverse of the average vertical water vapour gradient around the 5.5 ppm isopleth which is 6 km/ppm. Multiplied with the uncertainty in the measured VMR this leads to an altitude uncertainty of 3.3 km for MIAWARA-C and 1.6 km for MLS. The propagation of the altitude uncertainty in the least square fit leads then to the uncertainty of the slope of the fit.

From the 5.5 ppm contour of the MIAWARA-C water vapour time series we got effective descent rates of 428±12 m/day, 404±12 m/day and 468±13 m/day (Fig. 7) for the years 2015, 2016 and 2017. The descent rates were also calculated for different isopleths. At 5 ppm the descent rates are within ±4 % of the results form the 5.5 ppm isopleth and at 6 ppm the descent rates are 2–12.5 % lower. From the zonal mean MLS water vapour time series we get descent rates of 478±2 m/day, 354±2m/day and 401±2m/day which deviates 12 %, -12 % and -14 % from MIAWARA-C. The models do however have an average discrepancy of +45 % for SD-WACCM and -20 % for ERA5.

The descent rates of trace species in the Arctic autumn have been estimated previously. In the mesosphere at 75 km Forkman et al. (2005) found a descent rate of up to 300 m/day from CO and H_2O measurements with ground-based microwave radiometers located at 60°N. The average descent rate from October to February in the lower mesosphere was determined from ACE-FTS CH_4 and H_2O measurements and is 175 m/day (Nassar et al., 2005). Funke et al. (2009) found CO descent rates of 350-400 m/day at 50–70 km in September and October from MIPAS satellite measurements.

Ryan et al. (2018) were assessing the ability to derive middle atmospheric descent rates from trace gas measurements. For CO they concluded that CO chemistry and dynamical processes other than vertical advection are not negligible and that the CO descent rate does not represent the mean descent of the atmosphere. Therefore Ryan et al. (2018) suggested to interpret the descent rate of trace species as an effective rate of vertical transport of this trace species. H_2O has a longer lifetime than CO at 50–70 km (Brasseur and Solomon, 2005) which makes it a more robust tracer. However the SD-WACCM simulations show that the average H_2O descent rate (628 m/day) is substantially smaller than the average velocity of the vertical wind (845 m/day). The vertical wind from SD-WACCM was averaged for the same altitude range and time periods where the H_2O descent rates have been calculated. This shows that the vertical wind is not the only responsible factor for the descent of the 5.5 ppm isopleth.

The large difference between the mesospheric H_2O descent rate from simulations and measurements seems to indicate that the models have difficulties to catch the autumn descent of H_2O at high latitudes. It is also seen in the increasing relative differences between models and measurements in autumn and spring (see Fig. 3) when air parcels are descending and rising respectively. In an intercomparison of SD-WACCM CO data with measurements from MLS and the ground based microwave radiometer KIMRA at Kiruna (68 ° N) SD-WACCM shows higher CO VMRs in autumn and spring at high altitudes (86 and 76 km) (Ryan et al., 2018). The CO VMR is increasing with altitude whereas the H_2O VMR is decreasing. Therefore too high CO and too low H_2O VMRs in autumn could indicate a too strong mesospheric descent within SD-WACCM. But also

difficulties with the H_2O and CO chemistry might play a role because in spring SD-WACCM CO and H_2O are both higher than the measurements.

7 Vortex shifts in winter 2017

From January to April 2017 water vapour showed several spikes in the mesosphere (see Fig. 1). Thereby the water vapour VMR in the mesosphere at 0.1 hPa is enhanced by 2 ppm for about 4–11 days. In Fig. 8 (top) the water vapour time series is shown and the black contour lines indicates when the polar vortex edge is right above Ny-Ålesund. It is evident that the enhancements in mesospheric water vapour coincide with the periods where the polar vortex is shifted away from Ny-Ålesund. In the ozone time series the shift of the vortex away from Ny-Ålesund is seen as an enhancement in stratospheric ozone of about 2.5 ppm in January (Fig. 8 middle). In March the ozone increases in the middle stratosphere are less clearly linked to these shifts as during the period of polar night. An analysis of Lagranto 3-day backward trajectories shows the latitudinal origin of the airmasses at Ny-Ålesund. During the shifts of the upper stratospheric and mesospheric vortex the airmasses arrive from the midlatitudes (Fig.8 bottom). From the zonal mean time series of ECMWF temperature and zonal wind we find that the first three shifts meet the criteria of a minor sudden stratospheric warming according to the definition mentioned in Sec. 8.

8 Major sudden stratospheric warmings of 2016 and 2018

In the years 2015–2018 two major sudden stratospheric warmings (SSW) with a split of the polar vortex took place. For the characterisation of the event as minor or major warming we follow the definition of the World Meteorological Organisation (WMO) as presented in McInturff (1978): A stratospheric warming is called minor if a significant temperature increase is observed (i.e., at least 25 K in a period of a week or less) at any stratospheric level in any area of the wintertime hemisphere and if the criteria for major warmings are not met. A stratospheric warming is major if, additionally to the temperature increase, at 10 hPa or below the latitudinal mean temperature increases poleward from 60° latitude and an associated circulation reversal is observed (i.e., mean eastward winds poleward of 60° latitude are succeeded by mean westward winds in the same area).

The following sections present an analysis of the two major SSWs of the years 2016 and 2018 as seen from the perspective of Ny-Ålesund. We present MLS temperature measurements and water vapour, ozone and zonal wind measurements from the ground-based microwave radiometers MIAWARA-C and GROMOS-C.

8.1 Major SSW of March 2016

The first major SSW which we observed at Ny-Ålesund took place in March 2016. Figure 9 shows the contour lines of the polar vortex at 10, 1 and 0.1 hPa. The polar vortex edge was derived from ECMWF geopotential height (GPH) and wind fields as the GPH contours with highest wind speed at a given pressure level (Scheiben et al., 2012). In the stratosphere at 10 hPa the polar vortex was elongated and shifted away from Ny-Ålesund on March 2 for the first time. It regained a circular shape on March 5 before it shifted away from the pole again on March 9 and splitted on March 15. In the mesosphere (1 and 0.1 hPa)

the vortex was shifted away from the pole too and it got the form of a horseshoe. Because the polar vortex did not reestablish after the SSW and the circulation directly went over to the summer anticyclone, the event is called a major stratospheric final warming (Manney and Lawrence, 2016).

Figure 10 shows temperature, zonal wind, water vapour and ozone during the SSW 2016 at Ny-Ålesund. The black lines indicate the dates in Fig. 9. At 10 hPa the warming started on March 4 and the temperature increased 60 K in 2 days. During the stratospheric warming the isentropes descended in the stratosphere which contributed to the observed temperature increase through adiabatic heating of the descending airmasses. In the mesosphere the isentropes were rising and the upwelling of air along the isentropes led to adiabatic cooling and a temperature decrease of 40 K was measured at 0.01 hPa. The wind profiles from GROMOS-C captured the reversal of the zonal wind from eastward to westward in the mesosphere on March 5. In the stratosphere the zonal wind was already eastward during February because at the latitude of Ny-Ålesund a slight shift of the polar vortex off the pole and towards Ny-Ålesund is enough to reverse the zonal wind.

When the polar vortex moved away from Ny-Ålesund on March 2 stratospheric ozone increased by 1.5 ppm because ozone rich air from the midlatitudes reached the polar region. In the water vapour time series an increase in the mesosphere and a decrease in the stratosphere was seen which corresponds to the vertical water vapour structure outside of the polar vortex.

8.2 Major SSW of February 2018

The second major stratospheric warming which we observed took place in February 2018. Figure 11 shows the contour of the polar vortex at different stages during the SSW. In the stratosphere the polar vortex was elongated on February 9 and then it splitted in two on February 11 and moved away from Ny-Ålesund. On February 13 also the mesospheric vortex moved off the pole and on February 26 the mesospheric vortex reestablished whereas in the stratosphere the vortex was still split.

Figure 12 shows temperature, zonal wind, water vapour and ozone during the SSW 2018 at Ny-Ålesund and the black lines indicate the dates in Fig. 11. The stratospheric temperature between 100 and 10 hPa increased almost at the same time by 35 K or more within 3 days. In the mesosphere the temperature decrease started already on February 6. The isentropes show that airmasses were rising in the mesosphere and descending in the stratosphere. With the sudden stratospheric warming the temperature distribution in the stratosphere and mesosphere was almost homogeneous in the whole altitude range and the stratopause was no longer clearly defined.

The zonal wind measurements show a lot of changes in direction as it depends on the position of the polar vortex. Ozone increased dramatically by 4 ppm reaching a VMR of 8 ppm in the stratosphere when the vortex splitted on February 10 and midlatitude air was brought to Ny-Ålesund. Ongoing meridional mixing brought again ozone rich air from the midlatitudes on February 25 and the ozone VMR increased again to 8 ppm. In the water vapour time series a VMR increase was already seen on February 1 which is followed by a descent similar to the water vapour descent observed during the formation of the polar vortex. The mesospheric water vapour increase was accompanied by a water vapour decrease in the upper stratosphere.

Atmos. Chem. Phys. Discuss., https://doi.org/10.5194/acp-2018-1299
Manuscript under review for journal Atmos. Chem. Phys.
Discussion started: 14 January 2019

8.3 Ozone and water vapour during SSWs

During the two major SSWs in 2016 and 2018 stratospheric ozone and mesospheric water vapour were enhanced at Ny-Ålesund. The ozone enhancement is in agreement with the results of a composite analysis of 20 major SSWs in the ERA interim reanalysis dataset who found an increase in the total ozone column in the Arctic region after an SSW (Hocke et al., 2015). In contrast to the Arctic, at midlatitudes observations of stratospheric ozone during the 2008 SSW showed an ozone depletion along with the temperature increase (Flury et al., 2009). The depletion was mainly attributed to the effects of higher temperatures on the ozone chemistry especially to a higher efficiency of the catalytic ozone destruction through NOx. At Ny-Ålesund the net chemical ozone production rate in the stratosphere, taken from SD-WACCM, is always negative during the periods when the 2 SSWs took place and the enhancements result therefore solely from transport of ozone rich midlatitude air to the pole.

The midlatitude air also brought moister air to the mesosphere at Ny-Ålesund whereas in the upper stratosphere water vapour decreased because midlatitude air is drier than vortex air at that altitude. The evolution of water vapour during SSWs has been observed from midlatitude sites in earlier studies. At sites in Europe an increase in mesospheric water vapour was measured during the SSWs in the years 2008, 2010, 2012 and 2013 (Flury et al., 2009; Straub et al., 2012; Tschanz and Kämpfer, 2015) whereas in South Korea water vapour was decreasing during the 2008 SSW (De Wachter et al., 2011). The descent rate after the 2018 SSW in the lower mesosphere was calculated as explained in Sec. 6 for the period March 1–15 and is 355 m/day. This is in agreement with estimates of the water vapour descent rates from Sodankylä which are 350 m/day in 2010, 364 m/day in 2012 and 315 m/day in 2013. From water vapour and methane measurements with SOFIE Bailey et al. (2014) find a descent rate of 345 m/days after the 2013 SSW at approximately 70° N and between 50 and 60 km altitude.

Straub et al. (2012) showed that descent rates estimated with MIAWARA-C water vapour time series at Sodankylä after an SSW are in agreement with Transformed Eulerian Mean (TEM) trajectories derived from SD-WACCM simulations and that therefore the effective descent rates of water vapour are an estimate for the atmospheric residual circulation. This is in contrast to Ryan et al. (2018) which assessed the ability to derive atmospheric descent rates from CO and found that in general after an SSW other processes affect the CO VMR more than vertical advection. However in the region between 67 and 57 km altitude and from about 10 to 40 days after the SSW 2009 the CO descent rate agrees to the vertical advection (Ryan et al., 2018, Fig. 8). This is the area where the Straub et al. (2012) fitted the 5.2 water vapour isopleth and it could explain the agreement of the water vapour descent rate from the 5.2 isopleth with TEM trajectories.

In contrast to the vortex shifts in 2017 (Sec. 7), where the polar airmasses were clearly separated from midlatitude air at the polar vortex edge, the polar vortex system broke down during the major SSWs 2016 and 2018 and mixing of the airmasses occurred. Lagranto 3-day backward trajectories showed a high variability in the latitudinal origin of the airmasses at Ny-Ålesund during the 2 major SSWs. After the 2018 SSW the mesospheric polar vortex recovered in the end of February which is seen in the latitudinal origin returning to values larger than 60°latitude.

Atmos. Chem. Phys. Discuss., https://doi.org/10.5194/acp-2018-1299
Manuscript under review for journal Atmos. Chem. Phys.
Discussion started: 14 January 2019

9 Periodicities

Planetary waves are global-scale, coherent perturbations in the atmospheric circulation. Interactions of the waves with the mean-flow influence the large-scale dynamics (Andrews et al., 1987) and are believed to be the main cause of SSWs (Matsuno, 1970). The dominant periods of planetary waves were found at about 2, 5, 10 and 16 days in datasets from ground based instruments and from satellites (e.g. Lainer et al. (2018); Pancheva et al. (2018); Tschanz and Kämpfer (2015); Forbes and Zhang (2015); Scheiben et al. (2014); Day and Mitchell (2010); Riggin et al. (2006)). These periods correspond to the numerically calculated periods of Rossby normal modes and Rossby-gravity waves (Salby, 1981). Because of the variability in their wave periods the waves are called quasi-2-day wave (Q2DW), quasi-5-day wave (Q5DW), quasi-10-day wave (Q10DW), and quasi-16-day wave (Q16DW).

Water vapour and ozone VMRs above Ny-Ålesund have been measured with a high time resolution and the time series are therefore well suited for an analysis of short term fluctuations in the Arctic middle atmosphere. For the spectral decomposition of the water vapour and ozone time series we chose a wavelet like approach. The time series are filtered with a digital non-recursive, zero-phase finite impulse response filter using a Hamming window whose length is 3 times the center period (Hocke and Kämpfer, 2008; Hocke, 2009). The advantage of a wavelet like approach is that it captures intermittent waves with non-persistent phase.

The time series were separately filtered at every pressure level and for periods of 1–17 days. Figure 13 shows the mean peak-to-peak amplitude of the filtered signal for the different periods and pressure levels. The amplitudes are averaged over 80 day intervals centered at summer and winter solstices of the years 2015–2018. For ozone the figure is only shown for summer because in winter the ozone time series had long gaps.

Remarkable is the summer 2016 where the water vapour time series shows high amplitudes for periods of about 2, 5 and 10 days in the mesosphere at 0.1–0.01 hPa and for a period of 16 days in the upper stratosphere which corresponds to the periods of all the dominant Rossby normal modes and the Rossby-gravity wave. Also in the following two summers the water vapour time series shows the largest amplitudes in the mesosphere. The periods where we see the largest amplitudes do however not so clearly correspond to the normal modes. In winter periodicities are found between 1 and 0.1 hPa and cover a larger altitude range than in summer. In the winter 2016/2017 a strong Q5DW is present which is not seen in the other years. A persistent feature in winter is a wave with a period of about 3 days which is not attributed to the quasi 2- or 5-day wave. In general we note a high interannual variability in the dominant periods of the waves whereas the general pattern of the wave periods is repeated. Below 10 hPa no periodicities are seen.

In the ozone time series periodicities are seen in the stratosphere and the amplitudes are lower than for water vapour. The ozone time series in summer show signatures of a Q16DW with periods of 12–19 days in the stratosphere at about 10 hPa. In summer 2016 a Q16DW is found at the same altitude as for water vapour.

Periodicities in the water vapour time series are mainly seen at 0.1–0.01 hPa during summer whereas in winter periodicities are seen throughout the mesosphere. This could be due to the different water vapour distributions in summer and winter. In winter water vapour has a strong negative gradient throughout the whole mesosphere whereas in summer the water vapour

maximum is slightly above the stratopause and the gradient in the mesosphere is weaker. Around its maximum water vapour is not a good tracer due to missing gradients (Lee et al., 2011). However the seasonal differences in the altitude distribution of the periodicities would also agree with the findings of Tschanz and Kämpfer (2015) and Pancheva et al. (2018). In water vapour and geopotential height data they found that the amplitudes of Q2DWs peak at higher altitudes in summer than in winter. Additionally Day et al. (2011) found from temperature data that the Q16DW is present throughout the mesosphere in winter whereas in summer it is present only below 30 km and above 70 km. This pattern can also be recognised in our water vapour dataset where we see very low wave activity around the stratopause (1–0.1 hPa) in summer for periods around 16 days and high activity in winter. The chemical lifetime of ozone in the summer stratosphere according to SD-WACCM is about 20-40 minutes which is shorter than the timescale of transport. Nevertheless periodicities are found in the ozone time series. They might result from temperature variabilities because of temperature dependent photochemistry (Moreira et al., 2016; Flury et al., 2009; Pendlebury et al., 2008). In the SD-WACCM datasets we see a positive correlation of ozone and temperature around 10 hPa in summer, however in the MLS temperature data of Ny-Ålesund no signature of a Q16DW was found.

10 Summary and Conclusions

Continuous observations of water vapour and ozone in the Arctic middle atmosphere are rare. We presented a 3-year long time series of middle atmospheric water vapour and ozone measurements in the Arctic. These unique datasets have been measured with the two ground-based microwave radiometers MIAWARA-C and GROMOS-C at the AWIPEV research base at Ny-Ålesund, Svalbard in the years 2015–2018. The datasets are characterized by a high time resolution in the order of hours.

The water vapour and ozone datasets were intercompared with measurements of MLS and ACE and with SD-WACCM and ERA5 simulations. Ozone data were additionally intercompared with measurements of the ozone radiometer OZORAM which is also located at Ny-Ålesund and with balloon borne ozone sonde measurements when there was a reasonable overlap in altitude. On average SD-WACCM and ACE are within ± 5 % of the MIAWARA-C water vapour measurements up to 0.1 hPa. The MLS measurements have however a constant offset to MIAWARA-C over the 3 years which is on average 10–15 % depending on altitude. In the stratosphere GROMOS-C shows good agreement with the other datasets during winter whereas in summer GROMOS-C measures up to 20 % higher ozone values than the other datasets. On average GROMOS-C profiles are mainly within 5 % of the other datasets up to 0.5 hPa (about 55 km).

During the 3 years of observation at Ny-Ålesund we measured water vapour, ozone and horizontal wind during dynamical events which are typical for the Arctic middle atmosphere. The descent rate of mesospheric water vapour within the polar vortex in autumn was determined in the years 2015–2017 at 0.3–0.02 hPa in the mesosphere. The average effective descent rate determined from MIAWARA-C water vapour is 435 m/day. With MLS zonal mean water vapour measurements a descent rate of 410 m/day was found. The models show an average discrepancy of +45 % for SD-WACCM and -20 % for ERA5 which reflects the deviation of the models from the measurements in autumn.

From January to April 2017 the vortex shifted away from Ny-Ålesund four times. The polar vortex strongly separated Arctic and midlatitude air which was seen in the sudden increases of mesospheric water vapour and stratospheric ozone as soon as

the polar vortex moved away from Ny-Ålesund. Trajectory calculations with LAGRANTO confirmed the midlatitude origin of the airmasses during the vortex shifts.

Two sudden stratospheric warmings took place in March 2016 and in February 2018. Enhancements in mesospheric water vapour and stratospheric ozone were observed and the wind reversal was captured in the GROMOS-C wind measurements. During the SSW in 2018 a 4 ppm increase of stratospheric ozone was observed. From SD-WACCM simulations we see that the stratospheric ozone enhancement is a purely dynamical effect. In contrast to the vortex shifts in 2017, where the polar airmasses were clearly separated from midlatitude air at the polar vortex edge, the polar vortex system broke down during the major SSWs 2016 and 2018 and mixing of the airmasses occurred. After the 2018 SSW the polar vortex reestablished and we determined the descent rate of water vapour which is 355 m/day for March 1–15.

The water vapour and ozone time series were bandpass filtered and signatures of Rossby normal modes and Rossby-gravity waves with periods of 2, 5, 10 and 16 days were found. In the water vapour time series we note an interannual variation of the dominant periods whereas the general patterns of the wave periods are repeated.

We will continue the monitoring of ozone and water vapour in the variable polar middle atmosphere above Ny-Ålesund.

Author contributions. FS was responsible for the ground-based ozone measurements with GROMOS-C, performed the data analysis and prepared the manuscript. BT was responsible for the water vapour measurements with MIAWARA-C and MP for the ozone measurements with OZORAM. RR performed the wind retrieval from the GROMOS-C ozone spectra. KH designed the filter algorithm and NK contributed to the interpretation of the results.

Competing interests. The authors declare that they have no conflict of interest.

Acknowledgements. Observations with MIAWARA-C and GROMOS-C in Ny-Ålesund are funded by the Swiss National Science Foundation under grant number 200020-160048. For partial funding of this work we acknowledge the BMBF Germany (project 01LG1214A) and German Research Foundation (DFG) SFB/TR 172 Arctic Amplification: Climate Relevant Atmospheric and Surface Processes, and Feedback Mechanisms (AC)3 in projects B06 and E02. We thank the electronics workshop of the IAP and the AWIPEV team for their support during the campaign. In addition, we thank the satellite teams for providing the Aura/MLS and ACE/FTS data.

References

Andrews, D., Leovy, C., and Holton, J.: Middle Atmosphere Dynamics, 40, Academic Press, San Diego, 1987.

Bailey, S. M., Thurairajah, B., Randall, C. E., Holt, L., Siskind, D. E., Harvey, V. L., Venkataramani, K., Hervig, M. E., Rong, P., and Russell, J. M.: A multi tracer analysis of thermosphere to stratosphere descent triggered by the 2013 Stratospheric Sudden Warming, Geophys. Res. Lett., 41, 5216–5222, https://doi.org/10.1002/2014GL059860, 2014.

Baldwin, M. P. and Dunkerton, T. J.: Stratospheric harbingers of anomalous weather regimes, Science, 294, 581–584, https://doi.org/10.1126/science.1063315, 2001.

Bernath, P. F.: The Atmospheric Chemistry Experiment (ACE), J. Quant. Spectrosc. Radiat. Transf., 186, 3–16, https://doi.org/10.1016/j.jqsrt.2016.04.006, 2017.

Boyd, I. S., Parrish, A. D., Froidevaux, L., von Clarmann, T., Kyrölä, E., Russell, J. M., and Zawodny, J. M.: Ground-based microwave ozone radiometer measurements compared with Aura-MLS v2.2 and other instruments at two Network for Detection of Atmospheric Composition Change sites, J. Geophys. Res. Atmos., 112, 1–10, https://doi.org/10.1029/2007JD008720, 2007.

Brakebusch, M., Randall, C. E., Kinnison, D. E., Tilmes, S., Santee, M. L., and Manney, G. L.: Evaluation of Whole Atmosphere Community Climate Model simulations of ozone during Arctic winter 2004 – 2005, J. Geophys. Res., 118, 2673–2688, https://doi.org/10.1002/jgrd.50226, 2013.

Brasseur, G. P. and Solomon, S.: Aeronomy of the middle atmosphere, Springer, Dordrecht, Netherlands, 2005.

Buehler, S. A., Eriksson, P., Kuhn, T., Engeln, A. V., and Verdes, C.: ARTS , the atmospheric radiative transfer simulator, J. Quant. Spectrosc. Radiat. Transf., 91, 65–93, https://doi.org/10.1016/j.jqsrt.2004.05.051, 2005.

Collins, W. D., Rasch, P. J., Boville, B. A., Hack, J. J., McCaa, J. R., Williamson, D. L., Briegleb, B. P., Bitz, C. M., Lin, S.-J., and Zhang, M.: The Formulation and Atmospheric Simulation of the Community Atmosphere Model Version 3 (CAM3), J. Clim., 19, 2144–2161, 2006.

Copernicus Climate Change Service (C3S): ERA5: Fifth generation of ECMWF atmospheric reanalyses of the global climate, https://cds.climate.copernicus.eu/cdsapp#!/home, 2017.

Day, K. A. and Mitchell, N. J.: The 16-day wave in the Arctic and Antarctic mesosphere and lower thermosphere, Atmos. Chem. Phys., 10, 1461–1472, https://doi.org/10.5194/acp-10-1461-2010, 2010.

Day, K. A., Hibbins, R. E., and Mitchell, N. J.: Aura MLS observations of the westward-propagating s=1, 16-day planetary wave in the stratosphere, mesosphere and lower thermosphere, Atmos. Chem. Phys., 11, 4149–4161, https://doi.org/10.5194/acp-11-4149-2011, 2011.

De Mazière, M., Thompson, A. M., Kurylo, M. J., Wild, J. D., Bernhard, G., Blumenstock, T., Braathen, G. O., Hannigan, J. W., Lambert, J.-C., Leblanc, T., McGee, T. J., Nedoluha, G., Petropavlovskikh, I., Seckmeyer, G., Simon, P. C., Steinbrecht, W., and Strahan, S. E.: The Network for the Detection of Atmospheric Composition Change (NDACC): history , status and perspectives, Atmos. Chem. Phys., 18, 4935–4964, 2018.

De Wachter, E., Hocke, K., Flury, T., Scheiben, D., Kämpfer, N., Ka, S., and Oh, J. J.: Signatures of the Sudden Stratospheric Warming events of January-February 2008 in Seoul, S. Korea, Adv. Sp. Res., 48, 1631–1637, https://doi.org/10.1016/j.asr.2011.08.002, 2011.

Denton, M. H., Kivi, R., Ulich, T., Rodger, C. J., Clilverd, M. A., Horne, R. B., and Kavanagh, A. J.: Solar proton events and stratospheric ozone depletion over northern Finland, J. Atmos. Solar-Terrestrial Phys., pp. 1–10, https://doi.org/10.1016/j.jastp.2017.07.003, http://dx.doi.org/10.1016/j.jastp.2017.07.003, 2017.

Denton, M. H., Kivi, R., Ulich, T., Clilverd, M. A., Rodger, C. J., and von der Gathen, P.: Northern Hemisphere Stratospheric Ozone Depletion Caused by Solar Proton Events: The Role of the Polar Vortex, Geophys. Res. Lett., 45, 2115–2124, https://doi.org/10.1002/2017GL075966, 2018.

Emmons, L. K., Walters, S., Hess, P. G., Lamarque, J.-F., Pfister, G. G., Fillmore, D., Granier, C., Guenther, A., Kinnison, D., Laepple, T., Orlando, J., Tie, X., Tyndall, G., Wiedinmyer, C., Baughcum, S. L., and Kloster, S.: Description and evaluation of the Model for Ozone and Related chemical Tracers , version 4 (MOZART-4), Geosci. Model Dev., 3, 43–67, 2010.

Eriksson, P., Jiménez, C., and Buehler, S. A.: Qpack , a general tool for instrument simulation and retrieval work, J. Quant. Spectrosc. Radiat. Transf., 91, 47–64, https://doi.org/10.1016/j.jqsrt.2004.05.050, 2005.

Eriksson, P., Buehler, S. A., Davis, C. P., Emde, C., and Lemke, O.: ARTS , the atmospheric radiative transfer simulator , version 2, J. Quant. Spectrosc. Radiat. Transf., 112, 1551–1558, https://doi.org/10.1016/j.jqsrt.2011.03.001, 2011.

Fernandez, S., Murk, A., and Kämpfer, N.: GROMOS-C, a novel ground based microwave radiometer for ozone measurement campaigns, Atmos. Meas. Tech., 8, 3001–3048, https://doi.org/10.5194/amt-8-2649-2015, 2015.

Fernandez, S., Rüfenacht, R., Kämpfer, N., Portafaix, T., and Posny, F.: Results from the validation campaign of the ozone radiometer GROMOS-C at the NDACC station of Réunion island, Atmos. Chem. Phys., 16, 7531–7543, https://doi.org/10.5194/acp-16-7531-2016, 2016.

Flury, T., Hocke, K., Haefele, A., Kämpfer, N., and Lehmann, R.: Ozone depletion, water vapor increase, and PSC generation at midlatitudes by the 2008 major stratospheric warming, J. Geophys. Res. Atmos., 114, 1–14, https://doi.org/10.1029/2009JD011940, 2009.

Forbes, J. M. and Zhang, X.: Quasi-10-day wave in the atmosphere, J. Geophys. Res., 120, 11,079–11,089, https://doi.org/10.1002/2015JD023327, 2015.

Forkman, P., Eriksson, P., Murtagh, D., and Espy, P.: Observing the vertical branch of the mesospheric circulation at latitude 60°N using ground-based measurements of CO and H2O, J. Geophys. Res., 110, D05 107, https://doi.org/10.1029/2004JD004916, 2005.

Funke, B., López-Puertas, M., García-Comas, M., Stiller, G. P., Von Clarmann, T., Höpfner, M., Glatthor, N., Grabowski, U., Kellmann, S., and Linden, A.: Carbon monoxide distributions from the upper troposphere to the mesosphere inferred from 4.7 μm non-local thermal equilibrium emissions measured by MIPAS on Envisat, Atmos. Chem. Phys., 9, 2387–2411, https://doi.org/10.5194/acp-9-2387-2009, 2009.

Funke, B., López-Puertas, M., Bermejo-Pantalen, D., García-Comas, M., Stiller, G. P., Von Clarmann, T., Kiefer, M., and Linden, A.: Evidence for dynamical coupling from the lower atmosphere to the thermosphere during a major stratospheric warming, Geophys. Res. Lett., 37, 1–5, https://doi.org/10.1029/2010GL043619, 2010.

Hersbach, H. and Dee, D.: ERA5 reanalysis is in production, ECMWF Newsl., 2016.

Hocke, K.: QBO in solar wind speed and its relation to ENSO, J. Atmos. Solar-Terrestrial Phys., 71, 216–220, https://doi.org/10.1016/j.jastp.2008.11.017, 2009.

Hocke, K. and Kämpfer, N.: Bispectral analysis of the long-term recording of surface pressure at Jakarta, J. Geophys. Res. Atmos., 113, 1–9, https://doi.org/10.1029/2007JD009356, 2008.

Hocke, K., Lainer, M., and Schanz, a.: Composite analysis of a major sudden stratospheric warming, Ann. Geophys. Commun., 33, 783–788, https://doi.org/10.5194/angeocom-33-783-2015, 2015.

Hocke, K., Schranz, F., Barras, E. M., Moreira, L., and Kämpfer, N.: An Atlantic streamer in stratospheric ozone observations and SD-WACCM simulation data, Atmos. Chem. Phys., 17, 3445–3452, https://doi.org/10.5194/acp-17-3445-2017, 2017.

Hoffmann, C. G., Kinnison, D. E., Garcia, R. R., Palm, M., Notholt, J., Raffalski, U., and Hochschild, G.: CO at 40 – 80 km above Kiruna observed by the ground-based microwave radiometer KIMRA and simulated by the Whole Atmosphere Community Climate Model, 12, 3261–3271, https://doi.org/10.5194/acp-12-3261-2012, 2012.

Lainer, M., Hocke, K., and Kämpfer, N.: Long-term observation of midlatitude quasi 2-day waves by a water vapor radiometer, Atmos. Chem. Phys., 18, 12 061–12 074, https://doi.org/10.5194/acp-18-12061-2018, 2018.

Lee, J. N., Wu, D. L., Manney, G. L., Schwartz, M. J., Lambert, A., Livesey, N. J., Minschwaner, K. R., Pumphrey, H. C., and Read, W. G.: Aura Microwave Limb Sounder observations of the polar middle atmosphere: Dynamics and transport of CO and H2O, J. Geophys. Res. Atmos., 116, 1–18, https://doi.org/10.1029/2010JD014608, 2011.

Liu, H. L. and Roble, R. G.: A study of a self-generated stratospheric sudden warming and its mesospheric-lower thermospheric impacts using the coupled TIME-GCM/CCM3, J. Geophys. Res. Atmos., 107, 1–18, https://doi.org/10.1029/2001JD001533, 2002.

Manney, G. L. and Lawrence, Z. D.: The major stratospheric final warming in 2016: dispersal of vortex air and termination of Arctic chemical ozone loss, Atmos. Chem. Phys., 16, 15 371–15 396, https://doi.org/10.5194/acp-16-15371-2016, 2016.

Marsh, D. R., Mills, M. J., Kinnison, D. E., Lamarque, J.-F., Calvo, N., and Polvani, L. M.: Climate Change from 1850 to 2005 Simulated in CESM1 (WACCM), J. Clim., 1, 7372–7391, https://doi.org/10.1175/JCLI-D-12-00558.1, 2013.

Matsuno, T.: Vertical propagation of stationary planetary waves in the winter northern hemisphere, J. Atmos. Sci., 27, 871–883, 1970.

McInturff, R. M.: Stratospheric warmings: Synoptic, dynamic and general-circulation aspects, Natl. Aeronaut. Sp. Adm. Sci. Tech. Inf. Off., http://hdl.handle.net/2060/19780010687, 1978.

Mevi, G., Muscari, G., Paolo Bertagnolio, P., Fiorucci, I., and Pace, G.: VESPA-22: A ground-based microwave spectrometer for long-term measurements of polar stratospheric water vapor, Atmos. Meas. Tech., 11, 1099–1117, https://doi.org/10.5194/amt-11-1099-2018, 2018.

Moreira, L., Hocke, K., Navas-Guzmán, F., Eckert, E., and Von Clarmann, T.: The natural oscillations in stratospheric ozone observed by the GROMOS microwave radiometer at the NDACC station Bern, Atmos. Chem. Phys., 16, 10 455–10 467, https://doi.org/10.5194/acp-16-10455-2016, 2016.

Müller, M., Neuber, R., Fierli, F., Hauchecorne, A., Vömel, H., and Oltmans, S. J.: Stratospheric water vapour as tracer for vortex filamentation in the arctic winter 2002/2003, Atmos. Chem. Phys., 3, 1991–1997, https://doi.org/10.5194/acp-3-1991-2003, 2003.

Nassar, R., Bernath, P. F., Boone, C. D., Manney, G. L., McLeod, S. D., Rinsland, C. P., Skelton, R., and Walker, K. A.: ACE-FTS measurements across the edge of the winter 2004 Arctic vortex, Geophys. Res. Lett., 32, 1–5, https://doi.org/10.1029/2005GL022671, 2005.

Nedoluha, G. E., Kiefer, M., Lossow, S., Gomez, R. M., Kämpfer, N., Lainer, M., Forkman, P., Christensen, O. M., Oh, J. J., Hartogh, P., Anderson, J., Bramstedt, K., Dinelli, B. M., Garcia-Comas, M., Hervig, M., Murtagh, D., Raspollini, P., Read, W. G., Rosenlof, K., Stiller, G. P., and Walker, K. A.: The SPARC water vapor assessment II : intercomparison of satellite and ground-based microwave measurements, Atmos. Chem. Phys., 17, 14 543–14 558, 2017.

Palm, M., Hoffmann, C. G., Golchert, S. H. W., and Notholt, J.: The ground-based MW radiometer OZORAM on Spitsbergen – description and status of stratospheric and mesospheric O3-measurements, Atmos. Meas. Tech., 3, 1533–1545, https://doi.org/10.5194/amt-3-1533-2010, http://www.atmos-meas-tech.net/3/1533/2010/, 2010.

Pancheva, D., Mukhtarov, P., and Siskind, D. E.: Climatology of the quasi-2-day waves observed in the MLS/Aura measurements (2005–2014), J. Atmos. Solar-Terrestrial Phys., 171, 210–224, https://doi.org/10.1016/j.jastp.2017.05.002, https://doi.org/10.1016/j.jastp.2017.05.002, 2018.

Pendlebury, D., Shepherd, T. G., Pritchard, M., and McLandress, C.: Normal mode Rossby waves and their effects on chemical composition in the late summer stratosphere, Atmos. Chem. Phys., 8, 1925–1935, https://doi.org/10.5194/acp-8-1925-2008, 2008.

Rienecker, M., Suarez, M., Todling, R., Bacmeister, J., Takacs, L., Liu, H.-C., Gu, W., Sienkiewicz, M., Koster, R., Gelaro, R., Stajner, I., and Nielsen, J.: The GEOS-5 Data Assimilation System — Documentation of Versions 5.0.1, 5.1.0, and 5.2.0, Tech. Rep. December, NASA Goddard Space Flight Center, Greenbelt, https://ntrs.nasa.gov/archive/nasa/casi.ntrs.nasa.gov/20120011955.pdf, 2008.

Riggin, D. M., Liu, H. L., Lieberman, R. S., Roble, R. G., Russell, J. M., Mertens, C. J., Mlynczak, M. G., Pancheva, D., Franke, S. J., Murayama, Y., Manson, A. H., Meek, C. E., and Vincent, R. A.: Observations of the 5-day wave in the mesosphere and lower thermosphere, J. Atmos. Solar-Terrestrial Phys., 68, 323–339, https://doi.org/10.1016/j.jastp.2005.05.010, 2006.

Rodgers, C. D.: Retrieval of atmospheric temperature and composition from remote measurements of thermal radiation, Rev. Geophys. Sp. Phys., 14, 609–624, https://doi.org/10.1029/RG014i004p00609, 1976.

Rüfenacht, R. and Kämpfer, N.: The importance of signals in the Doppler broadening range for middle-atmospheric microwave wind and ozone radiometry, J. Quant. Spectrosc. Radiat. Transf., 199, 77–88, https://doi.org/10.1016/j.jqsrt.2017.05.028, 2017.

Rüfenacht, R., Kämpfer, N., and Murk, A.: First middle-atmospheric zonal wind profile measurements with a new ground-based microwave Doppler-spectro-radiometer, Atmos. Meas. Tech., 5, 2647–2659, https://doi.org/10.5194/amt-5-2647-2012, 2012.

Ryan, N. J., Kinnison, D. E., Garcia, R. R., Hoffmann, C. G., Palm, M., Raffalski, U., and Notholt, J.: Assessing the ability to derive rates of polar middle-atmospheric descent using trace gas measurements from remote sensors, Atmos. Chem. Phys., 18, 1457–1474, https://doi.org/10.5194/acp-18-1457-2018, 2018.

Salby, M. L.: Rossby normal modes in nonuniform background configurations. Part II: Equinox and solstice condition, Am. Meteorol. Soc., pp. 1827–1840, https://doi.org/10.1007/978-1-4614-3872-4_54, 1981.

Scheiben, D., Straub, C., Hocke, K., Forkman, P., and Kämpfer, N.: Observations of middle atmospheric H2O and O3 during the 2010 major sudden stratospheric warming by a network of microwave radiometers, Atmos. Chem. Phys., pp. 7753–7765, https://doi.org/10.5194/acp-12-7753-2012, 2012.

Scheiben, D., Tschanz, B., Hocke, K., Kämpfer, N., Ka, S., and Oh, J. J.: The quasi 16-day wave in mesospheric water vapor during boreal winter 2011/2012, Atmos. Chem. Phys., 14, 6511–6522, https://doi.org/10.5194/acp-14-6511-2014, 2014.

Schranz, F., Fernandez, S., Kämpfer, N., and Palm, M.: Diurnal variation in middle atmospheric ozone by ground based microwave radiometry at Ny-Ålesund over 1 year, Atmos. Chem. Phys., 18, 4113–4130, https://doi.org/10.5194/acp-2017-1080, 2018.

Sheese, P. E., Walker, K. A., Boone, C. D., Bernath, P. F., Froidevaux, L., Funke, B., Raspollini, P., and Clarmann, T. V.: ACE-FTS ozone , water vapour , nitrous oxide , nitric acid , and carbon monoxide profile comparisons with MIPAS and MLS, J. Quant. Spectrosc. Radiat. Transf., 186, 63–80, https://doi.org/10.1016/j.jqsrt.2016.06.026, 2017.

Straub, C., Murk, A., and Kämpfer, N.: MIAWARA-C, a new ground based water vapour radiometer for measurement campaigns, Atmos. Meas. Tech., 3, 1–20, https://doi.org/10.5194/amt-3-1-2010, 2010.

Straub, C., Tschanz, B., Hocke, K., Kämpfer, N., and Smith, A. K.: Transport of mesospheric H2O during and after the stratospheric sudden warming of January 2010: Observation and simulation, Atmos. Chem. Phys., 12, 5413–5427, https://doi.org/10.5194/acp-12-5413-2012, 2012.

Tschanz, B. and Kämpfer, N.: Signatures of the 2-day wave and sudden stratospheric warmings in Arctic water vapour observed by ground-based microwave radiometry, Atmos. Chem. Phys., 15, 5099–5108, https://doi.org/10.5194/acp-15-5099-2015, 2015.

Tschanz, B., Straub, C., Scheiben, D., Walker, K. A., Stiller, G. P., and Kämpfer, N.: Validation of middle-atmospheric campaign-based water vapour measured by the ground-based microwave radiometer MIAWARA-C, 6, 1725–1745, https://doi.org/10.5194/amt-6-1725-2013, 2013.

Waters, J. W., Froidevaux, L., Harwood, R. S., Jarnot, R. F., Pickett, H. M., Read, W. G., Siegel, P. H., Cofield, R. E., Filipiak, M. J., Flower, D. A., Holden, J. R., Lau, G. K., Livesey, N. J., Manney, G. L., Pumphrey, H. C., Santee, M. L., Wu, D. L., Cuddy, D. T., Lay, R. R., Loo, M. S., Perun, V. S., Schwartz, M. J., Stek, P. C., Thurstans, R. P., Boyles, M. A., Chandra, K. M., Chavez, M. C., Chen, G.-S., Chudasama, B. V., Dodge, R., Fuller, R. A., Girard, M. A., Jiang, J. H., Jiang, Y., Knosp, B. W., Labelle, R. C., Lam, J. C., Lee, K. A., Miller, D., Oswald, J. E., Patel, N. C., Pukala, D. M., Quintero, O., Scaff, D. M., Snyder, W. V., Tope, M. C., Wagner, P. A., and Walch, M. J.: The Earth Observing System Microwave Limb Sounder (EOS MLS) on the Aura Satellite, IEEE Trans. Geosci. Remote Sens., 44, 1075–1092, 2006.

Atmos. Chem. Phys. Discuss., https://doi.org/10.5194/acp-2018-1299
Manuscript under review for journal Atmos. Chem. Phys.
Discussion started: 14 January 2019

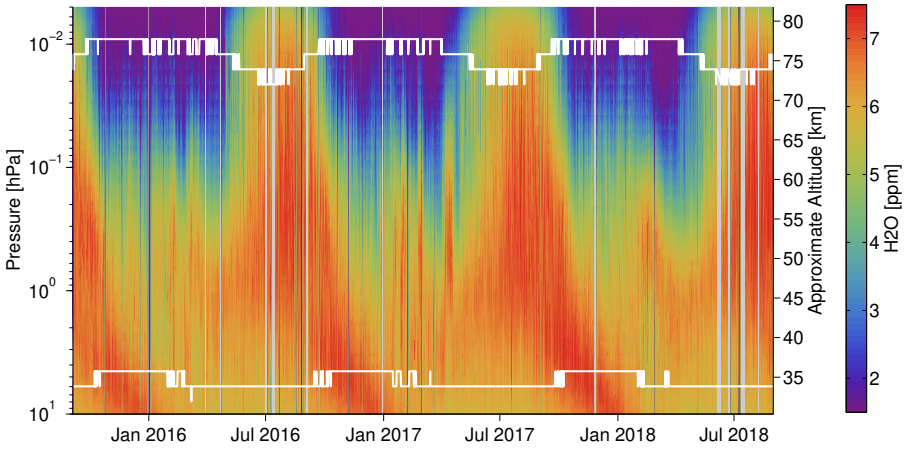

Figure 1. Time series of MIAWARA-C water vapour profiles from Ny-Ålesund. The horizontal white lines indicate the measurement response of 0.8.

Atmos. Chem. Phys. Discuss., https://doi.org/10.5194/acp-2018-1299
Manuscript under review for journal Atmos. Chem. Phys.
Discussion started: 14 January 2019

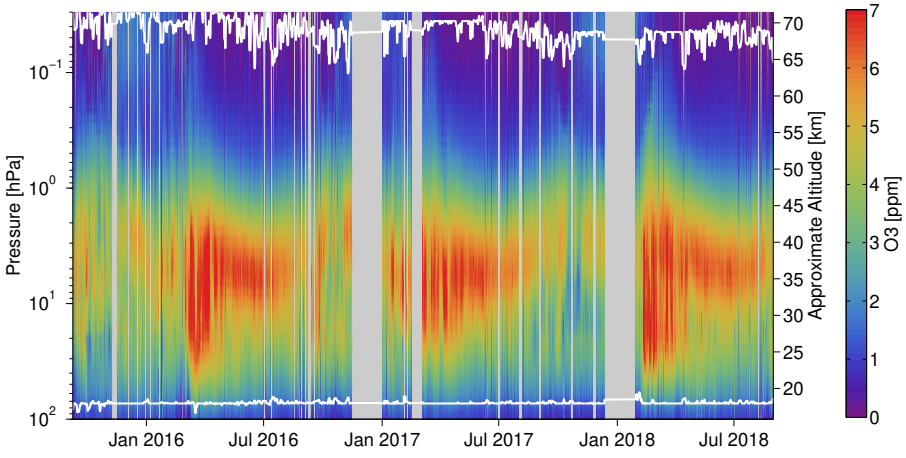

Figure 2. Time series of GROMOS-C ozone profiles from Ny-Ålesund. The horizontal white lines indicate the measurement response of 0.8.

Atmos. Chem. Phys. Discuss., https://doi.org/10.5194/acp-2018-1299
Manuscript under review for journal Atmos. Chem. Phys.
Discussion started: 14 January 2019

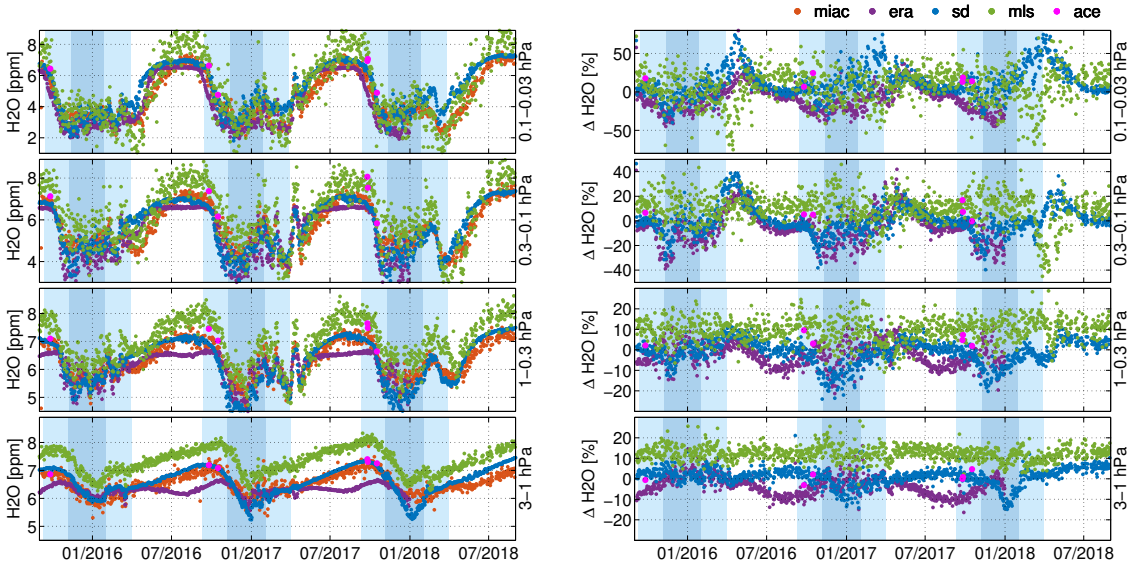

Figure 3. Intercomparison of water vapour time series at Ny-Ålesund. On the left are water vapour VMR time series of MIAWARA-C, MLS, ACE-FTS, SD-WACCM and ERA5 averaged within 4 pressure intervals where the upper 3 intervals are in the mesosphere and the lowest interval is in the upper stratosphere. On the right the relative differences to MIAWARA-C are shown for the same pressure intervals. The dark blue background indicates polar night and the white background polar day.

Atmos. Chem. Phys. Discuss., https://doi.org/10.5194/acp-2018-1299
Manuscript under review for journal Atmos. Chem. Phys.
Discussion started: 14 January 2019

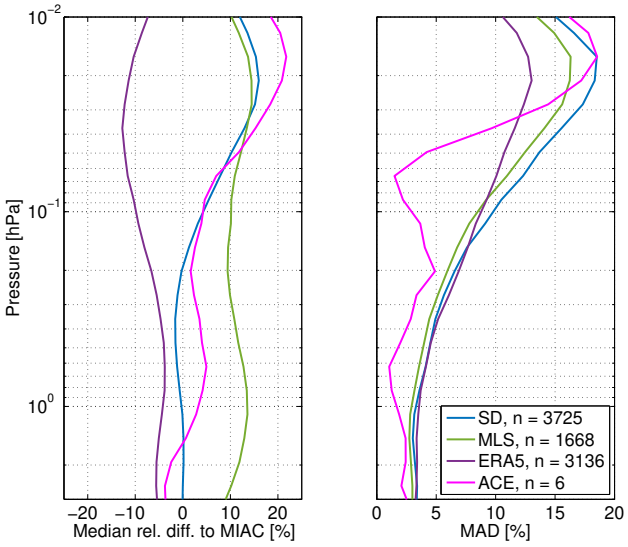

Figure 4. Median of the relative difference of SD-WACCM, MLS, ERA5 and ACE water vapour profiles and MIAWARA-C measurements at Ny-Ålesund (left). Median absolute deviation of the relative difference profiles (right). In the legend n indicates the number of coincident MIAWARA-C profiles.

Atmos. Chem. Phys. Discuss., https://doi.org/10.5194/acp-2018-1299
Manuscript under review for journal Atmos. Chem. Phys.
Discussion started: 14 January 2019

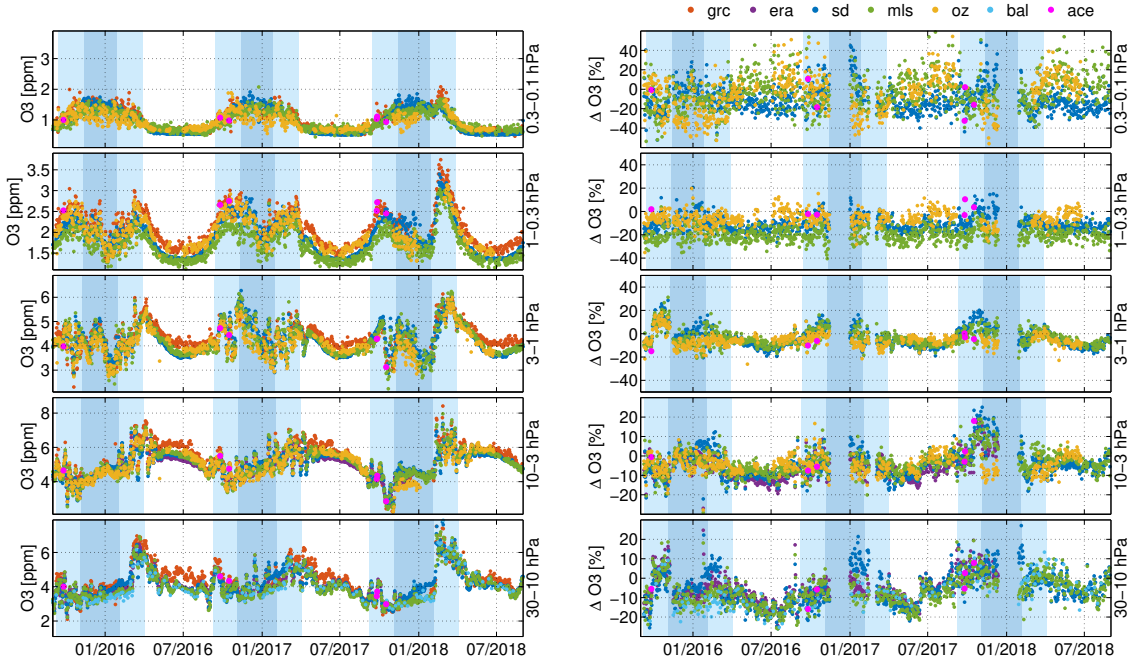

Figure 5. Intercomparison of ozone time series at Ny-Ålesund. On the left are ozone VMR time series of GROMOS-C, OZORAM, ozone sonde, MLS, ACE-FTS, SD-WACCM and ERA5 averaged within 5 pressure intervals where the lower 3 intervals are in the stratosphere and the upper 2 intervals are in the mesosphere. On the right the relative differences to GROMOS-C are shown for the same pressure intervals. The dark blue background indicates polar night and the white background polar day.

Atmos. Chem. Phys. Discuss., https://doi.org/10.5194/acp-2018-1299
Manuscript under review for journal Atmos. Chem. Phys.
Discussion started: 14 January 2019

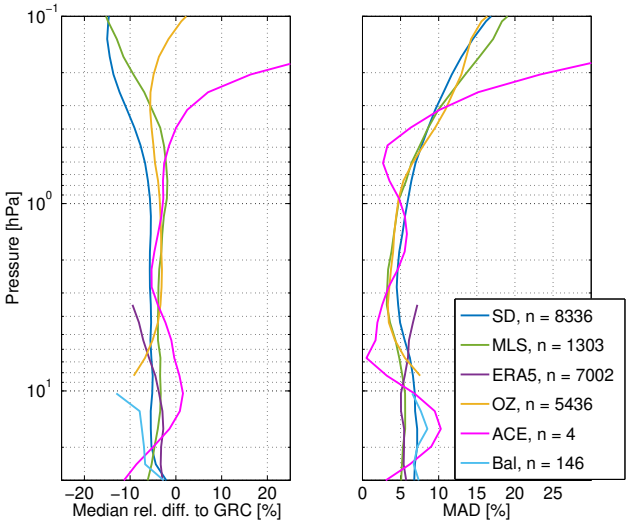

Figure 6. Median of the relative difference of SD-WACCM, MLS, ERA5, OZORAM, ACE and balloon-borne ozone sonde profiles and GROMOS-C ozone measurements at Ny-Ålesund (left). Median absolute deviation of the relative difference profiles (right). In the legend n indicates the number of coincident GROMOS-C profiles.

Atmos. Chem. Phys. Discuss., https://doi.org/10.5194/acp-2018-1299
Manuscript under review for journal Atmos. Chem. Phys.
Discussion started: 14 January 2019

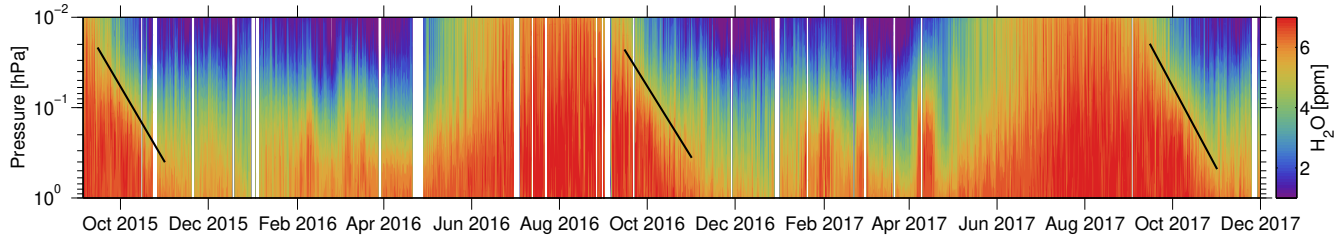

Figure 7. MIAWARA-C water vapour time series 2015–2017. The black line indicates the descent rate of water vapour within the polar vortex as derived from a linear fit of the 5.5 ppm isopleth. The descent rates are 428 m/day for 2015, 404 m/day for 2016 and 468 m/day for 2017.

Atmos. Chem. Phys. Discuss., https://doi.org/10.5194/acp-2018-1299
Manuscript under review for journal Atmos. Chem. Phys.
Discussion started: 14 January 2019

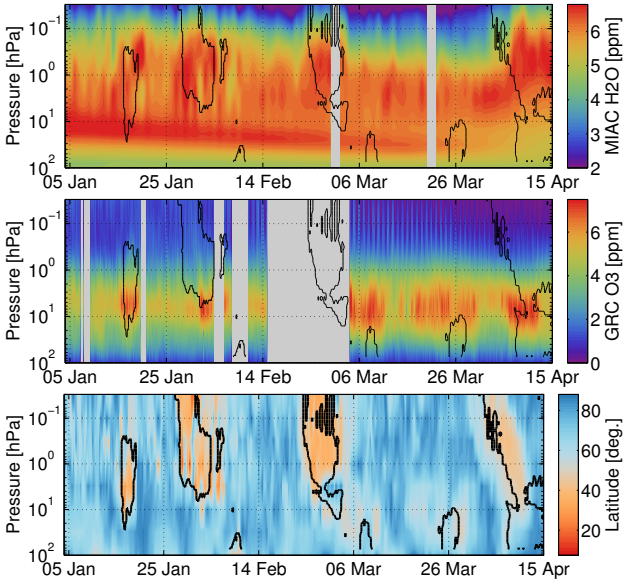

Figure 8. Time series of MIAWARA-C water vapour, GROMOS-C ozone and latitudinal origin of the air at Ny-Ålesund calculated with LAGRANTO 3-day backward trajectories. The black contours indicate when the polar vortex edge is above Ny-Ålesund. When the polar vortex shifts away from Ny-Ålesund water vapour and ozone increases are measured because airmasses arrive from the midlatitudes.

Atmos. Chem. Phys. Discuss., https://doi.org/10.5194/acp-2018-1299
Manuscript under review for journal Atmos. Chem. Phys.
Discussion started: 14 January 2019

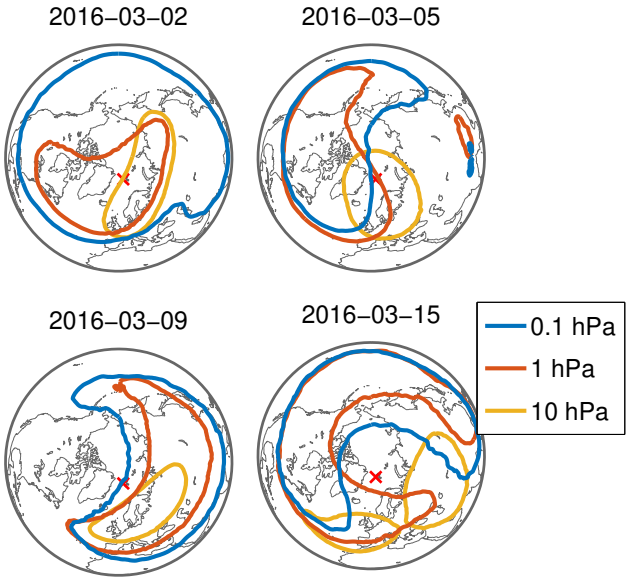

Figure 9. Contour lines of the polar vortex at 10 hPa, 1 hPa and 0.1 hPa during the major SSW of 2016. The red cross indicates the location of Ny-Ålesund.

Atmos. Chem. Phys. Discuss., https://doi.org/10.5194/acp-2018-1299
Manuscript under review for journal Atmos. Chem. Phys.
Discussion started: 14 January 2019

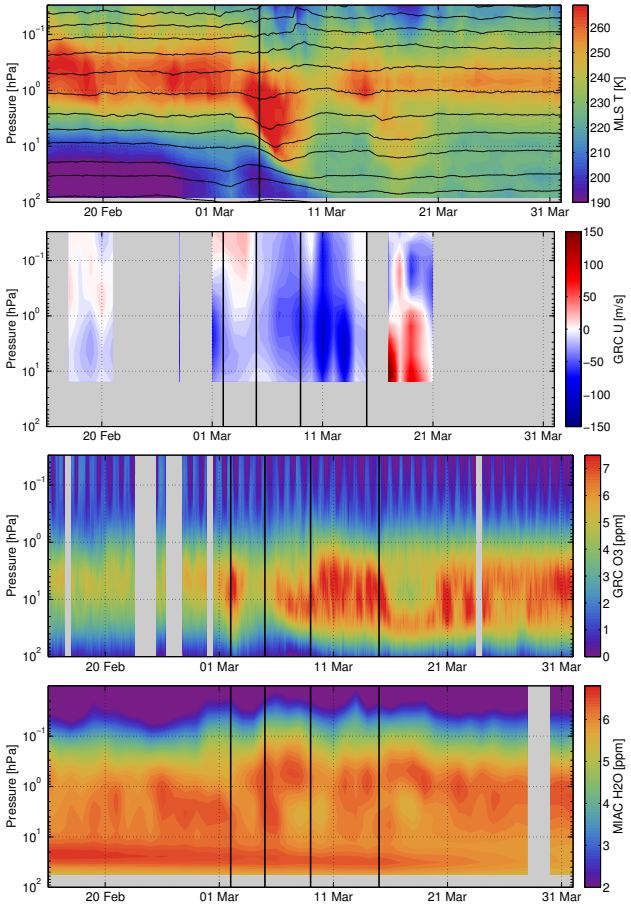

Figure 10. Time series of MLS temperature with isolines of potential temperature (solid black lines), GROMOS-C zonal wind, GROMOS-C ozone and MIAWARA-C water vapour during the SSW 2016 at Ny-Ålesund.

Atmos. Chem. Phys. Discuss., https://doi.org/10.5194/acp-2018-1299
Manuscript under review for journal Atmos. Chem. Phys.
Discussion started: 14 January 2019

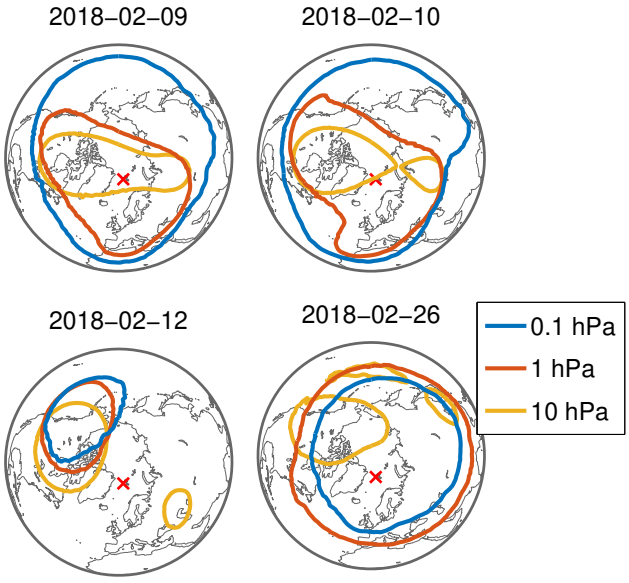

Figure 11. Contour lines of the polar vortex at 10 hPa, 1 hPa and 0.1 hPa during the major SSW of 2018. The red cross indicates the location of Ny-Ålesund.

Atmos. Chem. Phys. Discuss., https://doi.org/10.5194/acp-2018-1299
Manuscript under review for journal Atmos. Chem. Phys.
Discussion started: 14 January 2019

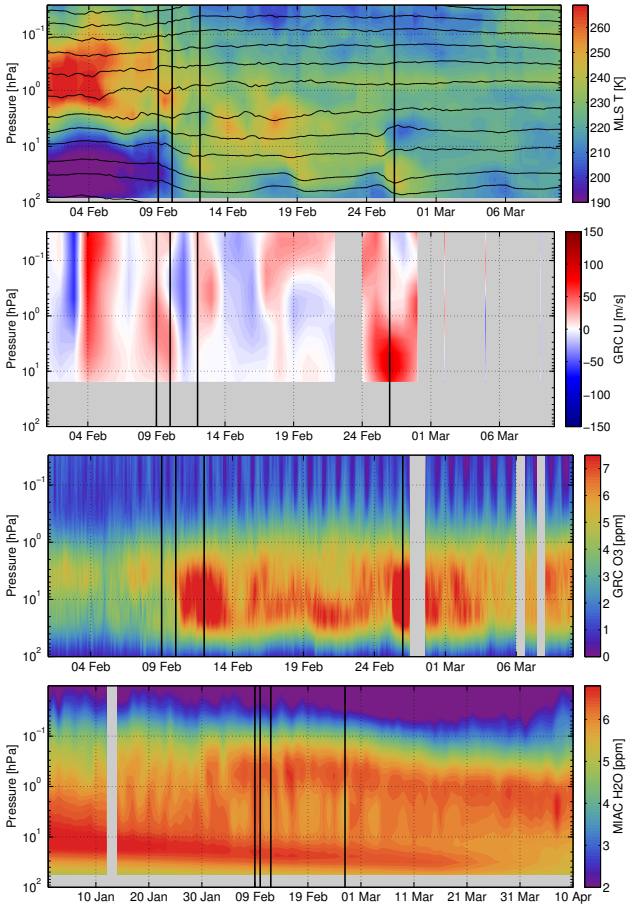

Figure 12. Time series of MLS temperature with isolines of potential temperature (solid black lines), GROMOS-C zonal wind, GROMOS-C ozone and MIAWARA-C water vapour during the SSW 2018 at Ny-Ålesund. Note the different time axis for the Water vapour time series.

Atmos. Chem. Phys. Discuss., https://doi.org/10.5194/acp-2018-1299
Manuscript under review for journal Atmos. Chem. Phys.
Discussion started: 14 January 2019

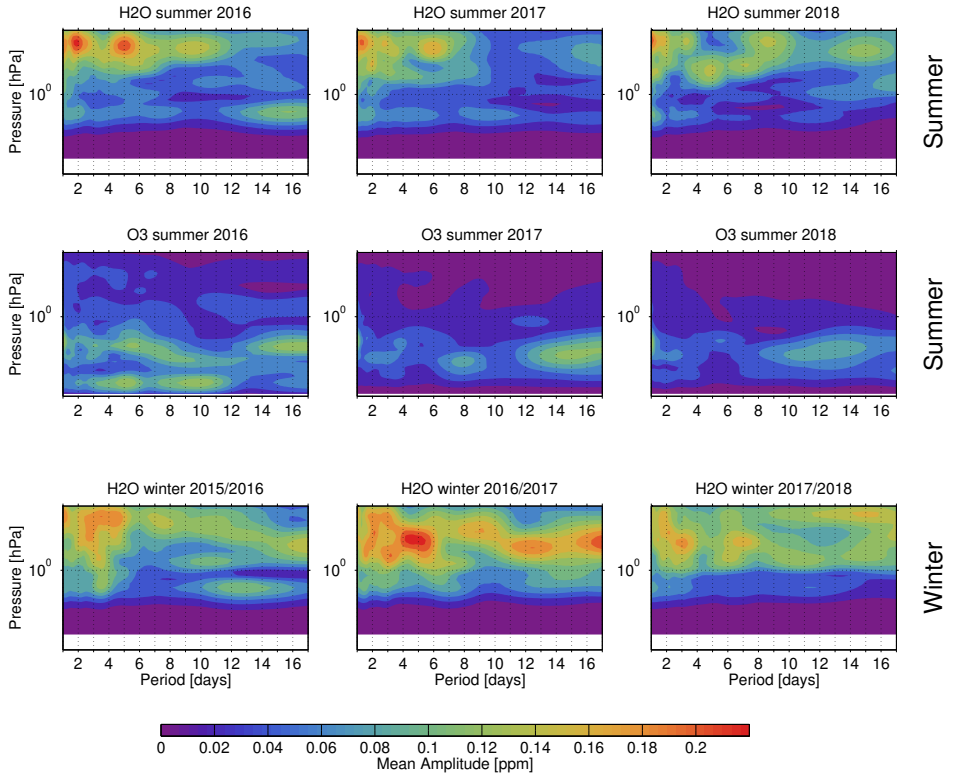

Figure 13. Mean amplitude for periods of 1–17 days obtained by bandpass filtering the water vapour and ozone time series for 80 day intervals centered around summer and winter solstice of the years 2015–2018.